Eur. Phys. J. D **18**, 113–121 (2002)
DOI: 10.1140/e10053-002-0013-8

THE EUROPEAN PHYSICAL JOURNAL D
EDP Sciences

An intense, slow and cold beam of metastable Ne(3s) $^3P_2$ atoms

J.G.C. Tempelaars, R.J.W. Stas, P.G.M. Sebel, H.C.W. Beijerinck, and E.J.D. Vredenbregt[a]

Physics Department, Eindhoven University of Technology, P.O. Box 513, 5600 MB Eindhoven, The Netherlands

Received 22 June 2001

Abstract. We employ laser cooling to intensify and cool an atomic beam of metastable Ne($3s$) atoms. Using several collimators, a slower and a compressor we achieve a $^{20}Ne^*$ flux of 6×10^{10} atoms/s in an 0.7 mm diameter beam traveling at 100 m/s, and having longitudinal and transverse temperatures of 25 mK and 300 μK, respectively. This constitutes the highest flux in a concentrated beam achieved to date with metastable rare gas atoms. We characterize the action of the various cooling stages in terms of their influence on the flux, diameter and divergence of the atomic beam. The brightness and brilliance achieved are 2.1×10^{21} $s^{-1}m^{-2}sr^{-1}$ and 5.0×10^{22} $s^{-1}m^{-2}sr^{-1}$, respectively, comparable to the highest values reported for alkali-metal beams. Bright beams of the ^{21}Ne and ^{22}Ne isotopes have also been created.

PACS. 39.25.+k Atom manipulation (scanning probe microscopy, laser cooling, etc.) – 32.80.Lg Mechanical effects of light on atoms, molecules, and ions – 32.80.Pj Optical cooling of atoms; trapping

1 Brightening rare-gas atomic beams

The efficiency with which metastable rare gas atoms can be produced in gas discharge sources is notoriously low, usually only on the order of 10^{-5} with the highest reported value being 10^{-3} for helium [1,2]. Traditionally, therefore, metastable rare gas atomic beams have shown much smaller flux and density than alkali-metal beams. In recent years, several groups [3–18] have tried to bridge this gap by employing laser cooling techniques [19] to intensify rare gas beams. At the same time, atomic beams could be made slow and monochromatic.

The principle of beam intensification using laser manipulation of atomic trajectories was illustrated by Sheehy *et al.* in a 1990 paper [20]. The essential element in any such scheme is a laser collimator, whose purpose is to increase the solid angle under which atoms can leave the source and still contribute to the beam flux further downstream. This is achieved by cooling the velocity component transverse to the atomic beam axis. The collimator completely determines the maximum gain in beam flux that can be obtained with laser cooling. Without collimation, the flux of atoms through a constant area decreases geometrically with its distance from the source; with collimation, this flux is essentially constant. Collimators for rare gas atomic beams have been employed by several groups [3–6,12–16,18].

Since transverse cooling takes a certain time and thus a certain transverse distance, laser collimation inevitably leads to large-diameter atomic beams whose density may be rather low despite the increased beam flux. The solution to this, according to reference [20], is to focus the beam and re-collimate it at the focal point. This idea was implemented in its purest form by Hoogerland *et al.* [3] who used a separate magneto-optical "lens" [21] (MOL) followed by a second collimator. Scholz *et al.* [7], Nellissen *et al.* [8] and Schiffer *et al.* [9] developed a magneto-optical compressor (MOC) in which both focusing and collimation occur within the same device. The mayor difference between a MOL and a MOC is the time spent within the device interacting with the laser fields: a compressor is basically a lens with a focal length shorter than the length of the interaction region. In order for the length of the MOC to stay within reasonable limits, laser slowing of the atomic beam [19,22] between collimator and compressor is necessary. A MOC device has since been applied to rare gas beams by Baldwin and coworkers [11,12] and by Koolen [4]. Koolen used a lens in combination with a compressor to increase the spatial capture range of the device. Labeyrie *et al.* [17] have also reported on the use of a MOL.

In this paper we describe our solution to brightening rare gas atomic beams, using all the devices mentioned above extended with additional cooling stages. This setup stands out because it produces the highest flux (6×10^{10} Ne($3s$) $^3P_2$ atoms/s) in a concentrated beam of any rare-gas atomic beam setup reported to date, comparable even to the brightest available alkali-metal beam [23].

[a] e-mail: E.J.D.Vredenbregt@TUE.nl

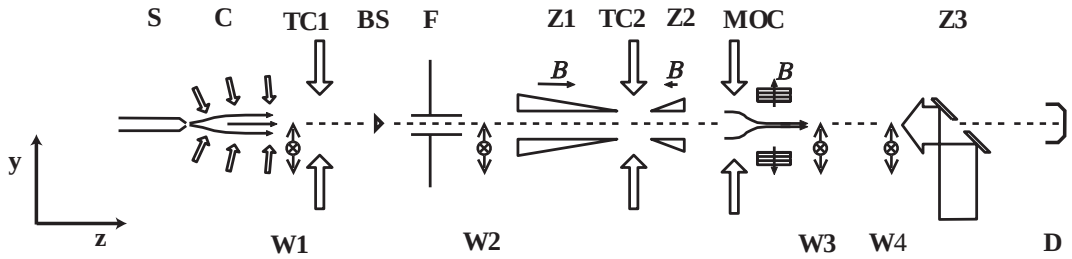

Fig. 1. Schematic overview of the beam line (not to scale) showing source, cooling stages, detectors and flow restriction. S: source, C: collimator, TC1, TC2, first and second transverse coolers; BS: beam stop (diameter 3 mm), F: flow restriction (150 mm × ϕ30 mm, Z1, Z2: tapered coils of Zeeman slower, Z3: 45° mirror with 3 mm diameter hole ("slower mirror"), MOC: magneto-optical compressor, D: beam flux detector, W1, W2, W3, W4: wire scanners.

2 Experimental setup

2.1 Overview

Figure 1 shows a schematic overview of the neon beam line, with five separate laser cooling stages used to create an intense beam of cold atoms. In all cooling stages we use the Ne($3s$) ^{3}P$_2$ $\leftrightarrow$ ($3p$) ^{3}D$_3$ optical transition at a wavelength $\lambda = 640.225$ nm. Important parameters for this transition are the linewidth $\Gamma = 8.5(2\pi)$ MHz, saturation intensity $I_\mathrm{s} = 42$ W/m^2 for circularly polarized and $I_\mathrm{s} = 72$ W/m^2 for linearly polarized light, recoil velocity $v_\mathrm{R} = 31$ mm/s and Doppler temperature $T_\mathrm{D} = 203$ μK [19].

First, a collimator captures metastable Ne($3s$) atoms from a discharge source and collimates them into a parallel beam. Then, an additional transverse cooling stage reduces the divergence of the beam to a few times the Doppler limit. In a Zeeman slower, the atoms are axially slowed to a velocity of 100 m s^{-1}. Again, an additional transverse cooling stage, positioned in between the two solenoids of the slower, reduces the divergence of the slowed atomic beam. Behind the slower, a magneto-optical compressor captures the slowed atoms and funnels them into a narrow beam, which then passes through a hole in a mirror and hits a detector that records the beam flux achieved. The total length of the beam line, taken from the nozzle of the discharge to the beam flux detector, is approximately 3.3 m.

Table 1 gives detailed information about the position and length of the different laser cooling stages and the position of detectors. We take the z-direction along the atomic beam axis.

2.2 Diagnostics

Four sets of wire scanners are positioned along the beam line for diagnostics. A wire scanner consists of a stainless steel wire that can be moved transversely through the atomic beam by a stepper motor. By scanning the wire through the atomic beam and measuring the current due to electrons emitted from the wire, a one-dimensional beam-current profile $I(x)$ is generated. The beam profile represents a line-integral over the two-dimensional density distribution $\Phi_m(x, y)$ of the atomic beam along the length l of the wire,

$$I(x) \approx \eta_\mathrm{A} e d_\mathrm{w} \int_{-l/2}^{l/2} \Phi_m(x, y)\mathrm{d}y, \qquad (1)$$

with η_A the Auger detection efficiency of the wire, e the elementary charge, and d_w the diameter of the wire. For scanners W1 and W2 in Figure 1, $l = 43$ mm and $d_\mathrm{w} = 1.0$ mm while for W3 and W4, $l = 60$ mm and $d_\mathrm{w} = 0.1$ mm.

Throughout this paper we use $\eta_\mathrm{A} = 1$ since the exact value of the quantum efficiency of the Auger process for Ne(^{3}P$_2$) atoms on metallic surfaces is not known (Hotop [24] reports $\eta_\mathrm{A} = 0.3{-}0.91$ for stainless steel); however, η_A is certainly less than 1 so that in this paper we effectively always report a lower limit for the atom flux.

The total flux $\dot{N}$ of metastable atoms in the beam at the position of a wire scanner is found by integrating $I(x)$ over the scan direction x. By comparing beam profiles taken with two successive scanners, information about the divergence of the atomic beam can be obtained. We calculate the divergence Θ of the atomic beam by dividing the difference in FWHM beam diameters d_i measured with the two wire scanners by their separation, $\Theta = (d_2 - d_1)/(z_2 - z_1)$.

Finally, on the way to a trapping chamber where the bright beam can be used, *e.g.*, for collision experiments or to load a magneto-optical trap [25], the atomic beam hits a conducting surface that can be moved in and out of the beam's path, which we use to measure the total useful atom flux.

2.3 Laser setup

All laser cooling stages are operated from a single continuous-wave single-frequency ring dye laser (Coherent 899-21) with a maximum output power of ≈ 1 W when pumped with 10 W of light from an Argon ion laser (Coherent Innova 315). We typically set the dye laser output to 700 mW; this is the output power used for the experiments reported here unless explicitly noted otherwise.

Table 1. Axial starting position z and length Δz of beam line components, with laser beam characteristics for the different cooling stages at a total laser output of 700 mW: total optical power used P, average on-resonance saturation parameter $\langle s_0 \rangle$ and laser detuning $\Delta_{\rm L}$.

Component	z (mm)	Δz (mm)	P (mW)	$\langle s_0 \rangle$ [a]	$\Delta_{\rm L}/\Gamma$
nozzle source	0				
collimator	43	150	4×20[b]	1.6	+8
1st wire scanner	210				
1st Doppler cooler	230	50	50	3.0	−1.8
beam stop	300				
flow restriction	390	100			
2nd wire scanner	790				
1st Zeeman solenoid	1 230	850	100	2.6	−50
2nd Doppler cooler	2 260	40	40	0.5	−1.8
2nd Zeeman solenoid	2 370	150	100	2.6	−50
MOC	2 670	90	250	1.9	−1.8
3rd wire scanner	2 800				
4th wire scanner	2 950				
slower mirror	3 000				
beam flux detector	3 320				

[a] For the Zeeman slower and MOC the light is circularly polarized while for the other stages it is linearly polarized.
[b] The collimator laser beam is split in two pairs of laser beams, one pair for cooling in the x-direction and one pair for cooling in the y-direction.

The laser is locked to a frequency that is shifted from the Ne ($3s$) ^{3}P$_2$ $\leftrightarrow$ ($3p$) ^{3}D$_3$ transition by using Zeeman-tuned saturated absorption spectroscopy. This "global detuning" $\Delta_{\rm L}$ of the dye laser is normally set at $\Delta_{\rm L} = -1.8\Gamma$ for reasons that will become apparent below. Beams for the various cooling stages are split off by combinations of half-wave plates and polarizing beam-splitter cubes. Two acousto-optic modulators (AOMs) are used to shift the laser frequency for the collimator (80 MHz AOM) and the Zeeman slower (400 MHz). Spherical and cylindrical telescopes are used to expand the laser beams to the required sizes; generally we expand a laser beam such that its FWHM diameters in the x- and y-directions approximately match the spatial extent of a cooling stage's interaction region; in this case the edges of the interaction region are irradiated at half the central intensity. Then, 50% of the power falls within the interaction area and the average intensity $\langle I \rangle$ is 72% of the peak value.

Table 1 gives details on the laser beam characteristics of each cooling stage.

2.4 Metastable atom source

The beam line starts with a liquid nitrogen cooled source that produces a beam of metastable ^{20}Ne($3s$) ^{3}P$_2$ atoms in a DC discharge that runs through the nozzle of a supersonic expansion. The average axial velocity of the atoms is 480 m/s with a FWHM width of 100 m/s (corresponding to a source temperature of 200 K and a longitudinal beam temperature of 4 K); the center-line intensity for ^{20}Ne($3s$) ^{3}P$_2$ atoms is 2×10^{14} s^{-1}sr^{-1}. Other high-energy products emerging from the source are atoms in the metastable ^{3}P$_0$ state, metastable atoms of the isotopes ^{21}Ne and ^{22}Ne, and UV photons.

2.5 Collimator

About 40 mm after the source, the atoms enter the collimator in which they are captured and collimated by a two-dimensional optical molasses [19]. For the molasses beams we use curved wave fronts to achieve a large capture angle while keeping the cooling time as short as possible. To minimize the required laser power, the curved wave fronts are produced by using the zig-zag method as we reported earlier [3]. Linearly polarized laser light is injected at an angle $\beta(\Delta z = 0)$ with respect to the plane perpendicular to the atomic beam axis between two 150 mm long, nearly parallel mirrors placed 60 mm apart. With each reflection, $\beta(\Delta z)$ is reduced by an amount $\alpha = 1.7$ mrad, the angle between the mirrors. The Doppler shift $\Delta_{\rm D}$ experienced by the atoms in the collimator is given by

$$\Delta_{\rm D} = -\mathbf{k} \cdot \mathbf{v} \approx -k v_{||} \beta + k v_{\perp}, \tag{2}$$

with $v_{||}$ and $v_{\perp}$ the longitudinal and transverse velocity of the atoms. With the condition $\Delta_{\rm D} + \Delta_{\rm L} = 0$ the resonant transverse velocity of the atoms is

$$v_{\perp}(\Delta z) = -\Delta_{\rm L}/k + v_{||} \beta(\Delta z). \tag{3}$$

At the entrance of the collimator this velocity is $v_{\perp}(\Delta z = 0) = 21$ m s^{-1} for the experimental parameters we use, *i.e.*,

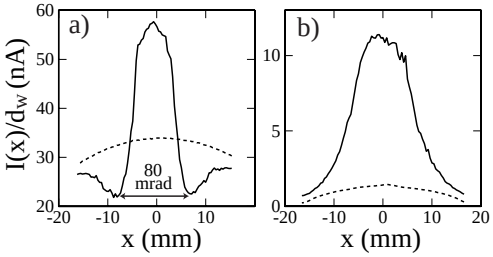

Fig. 2. Experimental spatial beam profiles behind collimating stage taken (a) just behind the collimator with wire scanner W1 and (b) 580 mm further downstream with wire scanner W2. Solid lines: cooling stages on; dashed lines: cooling stages off. The apparent loss in flux for the dashed lines between (a) and (b) is due to the influence of the flow resistance (see Fig. 1).

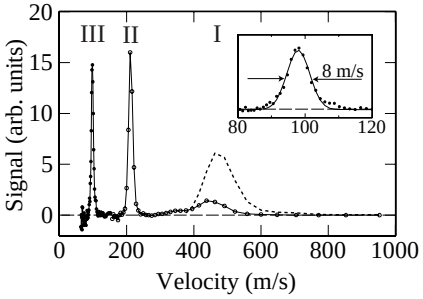

Fig. 3. Measured time-of-flight velocity distributions for unslowed (region I; dashed line), partially slowed (II; open circles) and fully slowed atoms (III; closed circles). The inset shows a Gaussian fit to the peak of fully slowed atoms, resulting in an 8.0 m/s FWHM velocity width.

$\beta(\Delta z = 0) = 130$ mrad and $\Delta_{\rm L} = +65\ (2\pi)$ MHz. This results in an FWHM capture angle $\Theta_{\rm c} = 2v_\perp/\bar{v}_{||} = 86$ mrad, corresponding to 7% of the source's FWHM divergence. At the end of the collimator at $\Delta z = 150$ mm, *i.e.*, after 12 reflections of the laser beam on each mirror, the resonance velocity is reduced to $v_\perp(\Delta z = 150\ {\rm mm}) = 2$ m/s. This effective detuning at the end of the collimator depends on the axial velocity of the atoms and thus does not provide the lowest possible divergence of the atomic beam. Therefore, an additional, short, transverse cooling stage is positioned immediately behind the collimator to further reduce the divergence of the atomic beam. Here we use $\Delta = -1.8\Gamma$ and $\beta = 0$; in-vacuum mirrors create the two-dimensional molasses from a single, linearly polarized laser beam.

Figure 2 shows experimental beam profiles taken in the x-direction with wire scanner W1 (which is placed just behind the collimator), and with scanner W2 placed 580 mm further downstream. The effect of the collimator is clearly visible: the atoms are captured and cooled in transverse direction, resulting in an atomic beam with a FWHM diameter of $d_{\rm col} = 9$ mm containing $\dot{N}_{\rm col} = 1.1 \times 10^{12}$ atoms/s in the $^3{\rm P}_2$ state. From the figure the capture angle of the collimator is estimated at $\Theta_{\rm c} = 80$ mrad, approximately the same as found with equation (3). The measurements with the second scanner then show a FWHM divergence of the beam of 10 mrad. This value could in principle be reduced further by changing the detuning of the transverse cooling stage; the detuning chosen is a compromise that leads to maximum overall output of the beam machine but which does not necessarily optimize each stage individually (we discuss this further in Sect. 3).

Switching the collimation and transverse cooling laser off, the beam flux decreases drastically, as shown by the dashed line in Figure 2b. This beam profile contains, besides atoms in the $^3{\rm P}_2$ state, also unwanted products of the source, *i.e.*, atoms in the metastable $^3{\rm P}_0$ state, metastable atoms of the other isotopes, and UV photons. Therefore a beam stop, consisting of a disc with a diameter of 3 mm, can be positioned in the center of the atomic beam just behind the transverse cooler (see Fig. 1). This beam stop keeps unwanted products (including ground state atoms) from reaching the end of the setup, while most of the laser cooled atoms ($\approx 90\%$ as follows from the ratio of the beam diameter to the diameter of the beam stop) pass around it, due to the different nature of the trajectories of cooled atoms *versus* uncooled atoms and UV photons. The mechanical beam stop was chosen over other means of separating unwanted products, such as laser deflection [5,7,10,15,26,27], for its extreme simplicity and ease.

2.6 Zeeman slower

The collimated atoms then pass through a flow restriction into a differential pumping region that allows for a reduction in background pressure (around 10^{-6} mbar in the collimation chamber due to the gas load from the source). Subsequently, the atoms enter a midfield-zero Zeeman slower [19,22] in which they are decelerated by a counter-propagating laser beam. The laser beam is coupled in by a mirror positioned in the vacuum behind the magneto-optical compressor (Z3 in Fig. 1). The atomic beam can pass through a 3 mm diameter hole in the center of this "slower mirror" since the compressor greatly reduces the beam's radius. The length of the slower is such that 10% of the maximum possible scattering force is sufficient to slow the atoms down. The tapered magnetic field coils (0.85 m and 0.15 m long) are usually set to produce maximum fields of 275 gauss and –175 gauss. In combination with the 400 MHz detuning of the circularly polarized slowing laser, this means that atoms with initial velocities up to 500 m/s should be slowed to a final velocity close to 100 m/s.

We measured the longitudinal velocity of the atoms leaving the Zeeman slower by a standard time-of-flight technique. Figure 3 shows the measured velocity distribution of unslowed, partially slowed (second Zeeman solenoid operated with reduced current), and fully slowed atoms. As expected, fully slowed atoms have a final velocity of 98 m/s. The measured FWHM width is 8.0 m/s in this case, corresponding to a longitudinal beam temperature of $T_{||} = 25$ mK.

During the slowing process the divergence of the atomic beam increases due to the reduction in axial

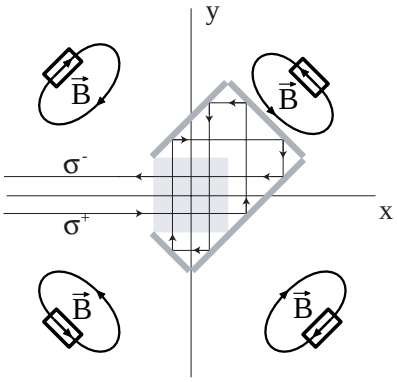

Fig. 4. Schematic cross-section of the magneto-optical compressor. In-vacuum mirrors create two pairs of σ^+/σ^- molasses beams. Four NdFeB magnets, positioned near the end of the mirrors, are arranged to create a quadrupole magnetic field whose strength increases along z.

velocity as well as the randomness in the direction of the spontaneously emitted photons. To counteract this effect, an additional transverse cooling stage is inserted between the two solenoids of the Zeeman slower. Transverse cooling is possible here because the magnetic field vanishes between the two solenoids. Here we use a simple "V"-shaped arrangement of two in-vacuum mirrors to create the two-dimensional molasses from a single, linearly polarized laser beam. Reducing the divergence of the atomic beam increases the flux of atoms within the capture range of the magneto optical compressor. We obtain a factor two increase in beam flux behind the MOC in this way.

2.7 Magneto-optical compressor

Behind the Zeeman slower, the atomic beam passes through a magneto-optic compressor to reduce its diameter and divergence. Figure 4 shows a schematic view of the device, which is basically a two-dimensional magneto-optic trap where the magnetic field gradient increases along the symmetry axis. Scholz *et al.* [7] have given a description of the motion of atoms inside a MOC.

Two pairs of $\sigma^+ - \sigma^-$ laser beams are produced by bouncing a single σ^+ laser beam on a set of in-vacuum mirrors. Atoms interact over a distance of $2w_z = 90$ mm with the laser beams, whose average on-resonance saturation parameter is $\langle s_0 \rangle = \langle I \rangle / I_\mathrm{s} = 1.9$ while the detuning $\Delta_\mathrm{L} = -1.8\Gamma$.

The magnetic quadrupole field of the MOC is generated by four permanent magnets mounted outside of the vacuum system near the end of the mirror arrangement. The NdFeB magnets have dimensions $60 \times 60 \times 30$ mm^3 and a magnetization of 1.15 T. At the entrance of the MOC a μ-metal shield helps to reduce the quadrupole field gradient to 0.1 T/m, which increases to 0.6 T/m at the end of the MOC. Given the initial field gradient and laser detuning, an initial resonance circle with radius $r_\mathrm{c} = -\Delta_\mathrm{L}/(\mu_\mathrm{B} \nabla B) = 10$ mm exists within which all atoms will be captured and funneled to the beam axis. Here, μ_B is the Bohr magneton.

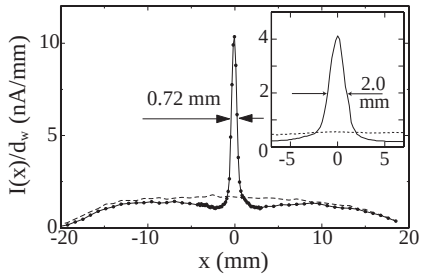

Fig. 5. Spatial beam profile measured immediately behind the compressor with wire scanner W3, showing a beam diameter $d = 0.72$ mm. The inset shows the profile 150 mm further downstream, measured with wire scanner W4. Solid lines, solid circles: compressor on; dashed line: compressor off.

Figure 5 shows beam profiles measured with the vertical wire of the third and fourth wire scanners. The effect of the MOC is very visible: atoms are molded into a narrow beam with a diameter of $d_\mathrm{MOC} = 0.72$ mm and a divergence of 8 mrad, containing $N_\mathrm{MOC} = 5 \times 10^{10}$ atoms/s. This results in a particle density of $n = 4\dot{N}/(\pi d^2 \bar{v}_{||}) = 1.2 \times 10^9$ cm^{-3}. From the figure it is also clear that many of the slowed atoms arrive outside the capture range of the MOC and cannot contribute to the flux of the compressed beam.

The measured FWHM divergence $\Delta v_\perp = 0.84$ m/s approximately corresponds to the FWHM transverse Doppler velocity $\Delta v_\mathrm{D} = 0.68$ m/s, resulting in a transverse beam temperature $T_\perp = 300$ μK. One might expect the transverse temperature to be lower than this value, since sub-Doppler cooling is possible when atoms are sufficiently near the beam axis at the end of the MOC [9]. We have found, however, that the final divergence is limited to approximately the Doppler value by a Stern-Gerlach effect. After the atoms exit the compressor's interaction region, they still have to traverse a large quadrupole field which exerts a force [4]

$$\mathbf{F}_\mathrm{SG} = (\boldsymbol{\mu} \cdot \boldsymbol{\nabla})\mathbf{B} = -\mu_\mathrm{B} g_\mathrm{g} m_\mathrm{g} \boldsymbol{\nabla} |B|, \qquad (4)$$

directed transverse to the beam axis, leading to motion away from the axis (this Stern-Gerlach force can be ignored inside the MOC because there the optical forces dominate). Here, m_g is the magnetic sublevel occupied by the atom when it leaves the compressor's interaction region and $g_\mathrm{g} = 1.5$ the Landé factor. We calculate that in our case Stern-Gerlach forces contribute around 4 mrad to the divergence of the atomic beam [28], effectively ruling out sub-Doppler transverse collimation. (Of course, further collimation is possible once outside the range of the quadrupole field.)

3 Overall performance

3.1 Detuning and intensity dependence

As mentioned earlier, the detuning used in the various stages is the result of a compromise that results from deriving all laser beams from a single source using a very

Table 2. Characteristics of the atomic beam. The total flux $\dot{N}$, FWHM diameter d, average longitudinal velocity $v_{||}$ and FWHM transverse velocity spread $\Delta v_\perp$, brightness $\mathcal{R}$, brilliance $\mathcal{B}$ and reduced phase-space density $\tilde{\Lambda}$ are given as measured at position z_m (second column) when the setup is operational up to the given cooling stage. The last three columns give the brightness, brilliance and phase-space density measured at the position of the flux detector ($z = 3\,320$ mm) when the setup is operational up to the given cooling stage, relative to the values for full operation.

stage	z_m	$\dot{N}$	d	$\bar{v}_{\|\|}$	$\Delta v_\perp$	$\mathcal{R}$	$\mathcal{B}$	$\tilde{\Lambda}$	$\mathcal{R}/\mathcal{R}_{\mathrm{All}}$	$\mathcal{B}/\mathcal{B}_{\mathrm{All}}$	$\tilde{\Lambda}/\tilde{\Lambda}_{\mathrm{All}}$
	mm	10^{10}/s	mm	m/s	m/s	10^{20}/ (s m^{2}sr)	10^{20}/ (s m^{2}sr)	10^{-13}			
source	0	2 600	0.15	480	580	130	1 250	580	4×10^{-7}	2×10^{-7}	3×10^{-10}
collimator	210	110	9	480	11	0.42	4.0	1.9	1×10^{-2}	5×10^{-3}	9×10^{-6}
1st Doppler cooler	790	110	15	480	4.8	0.79	7.6	3.5	3×10^{-1}	1×10^{-1}	2×10^{-4}
Zeeman slower	2 800	55[a]	30[a]	98	2.0[a]	0.01	0.26	70	1×10^{-2}	1×10^{-2}	1×10^{-2}
MOC	2 800	4.8	0.72	98	0.84	21	500	1.3×10^{6}	1	1	1

[a] Approximate values.

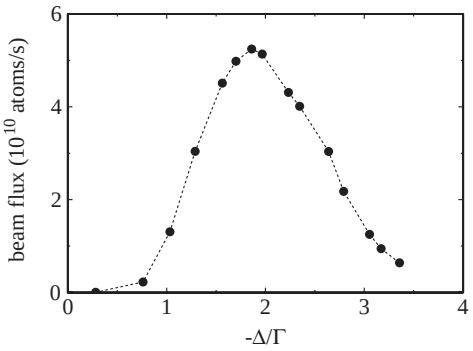

Fig. 6. Dependence of the total beam flux on the central detuning of the dye laser, showing maximum output at $\Delta_{\mathrm{L}} = -1.8\Gamma$.

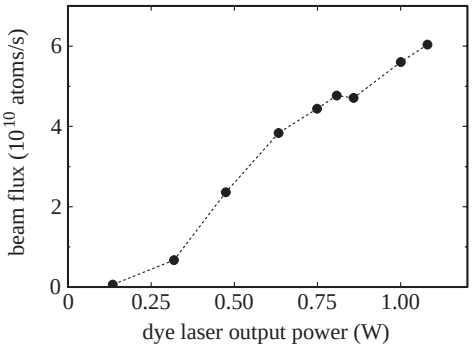

Fig. 7. Dependence of the total beam flux on the output power of the dye laser at a central detuning $\Delta = -1.8\Gamma$.

limited amount of AOMs. In Figure 6 we show the dependence of the beam flux as measured behind the slower mirror on the overall detuning of the dye laser. A fairly sharp maximum appears at $\Delta = -1.8\Gamma$, which was consequently chosen as the working point for the setup.

A similar compromise is necessary in order to fix the distribution of optical power over the various cooling stages. In general, all of these show increased performance with the on-resonance saturation parameter s_0 up to at least $s_0 = 2$, requiring more than the nominal output of the dye laser to attain everywhere. The distribution of power apparent in Table 1 is therefore the result of much empirical work. Figure 7 shows the dependence of the output of the beam machine on the total laser power available from the dye laser. The figure shows that the output of the setup increases with laser power in the entire range accessible to us. Consequently, we achieve the maximum beam flux of 6×10^{10} metastable ^{20}Ne atom/s at the maximum available laser output power of 1 W.

3.2 Brightness and brilliance

In the previous sections we showed that, by using several sets of wire scanners, it is possible to measure the characteristics of the atomic beam such as the flux $\dot{N}$ of atoms, the beam diameter and divergence. These quantities can be summarized into values for the brightness $\mathcal{R}$, brilliance $\mathcal{B}$ and reduced phase-space density $\tilde{\Lambda}$ of the atomic beam. Following Lison *et al.* [23],

$$\mathcal{R} = \frac{4\dot{N}}{\pi d^2 \Omega}, \tag{5}$$

$$\mathcal{B} = \mathcal{R}\frac{2\bar{v}_{||}}{\Delta v_{||}}, \tag{6}$$

$$\tilde{\Lambda} = \mathcal{B}\frac{\pi h^3}{m^3 v_{||}^4}, \tag{7}$$

where $\Delta v_{||}$ is the longitudinal velocity spread and Ω the geometric solid angle occupied by the beam, $\Omega = \pi(\Delta v_\perp / 2\bar{v}_{||})^2$, with $\Delta v_\perp$ and $v_{||}$ the FWHM transverse velocity spread and average longitudinal velocity of the atoms, respectively [29].

Table 2 lists measured beam characteristics such as beam flux, beam diameter, longitudinal and transverse velocities, as well as *local* values of the brightness, brilliance and reduced phase space density calculated from these. Looking at the measured beam flux, going from the collimator to the end of the setup, about a factor of 20 in beam

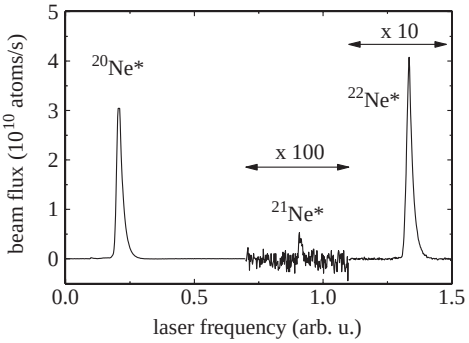

Fig. 8. Total beam flux recorded during $\approx$ 2 GHz wide scan of dye laser frequency. All three stable isotopes of neon are observed with relative rates of ^{20}Ne*:^{21}Ne*:^{22}Ne* = 1:0.0011:0.12. (Note dual scale change on vertical axis.)

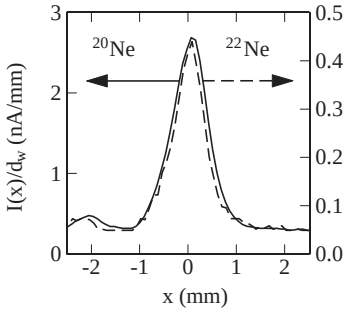

Fig. 9. Spatial beam profiles for ^{20}Ne* (solid line, left vertical axis) and ^{22}Ne* (dashed line, right vertical axis) taken with wire scanner W3 at a central detuning $\Delta = -1.8\Gamma$.

flux is lost. This is mostly caused by the fact that only a small fraction of the slowed atoms can be captured by the magneto-optical compressor, due to its limited spatial capture range in combination with the rather large diameter and divergence of the atomic beam leaving the slower. This effect could be remedied somewhat by using an additional MOL between slower and MOC [4]. Also, experiments show that the slower only slows a fraction of $\approx 50\%$ of the atoms that enter it to 100 m/s, probably due to imperfections in the slowing laser's beam profile as well as imperfect optical pumping into the $m_g = 2$ magnetic sub-level at the start of the slowing process.

The brightness and brilliance of the atomic beam increase drastically going from source to compressor. This is clear from the last three columns of Table 2, which give the values of the brightness, brilliance and reduced phase space density at the end of the setup for different operation modes of the atomic beam machine, going from limited operation (source only) to full operation (all laser cooling stages on). Switching on the slower greatly decreases brightness and brilliance due to the increasing beam diameter and divergence; the magneto-optical compressor compensates for this loss. Comparing the operation with only the source on to the full operation mode, we see that the brightness and brilliance increase six to seven orders of magnitude and the phase-space density nine orders of magnitude. Regrettably, the latter is still seven orders of magnitude from the quantum limit $\tilde{\Lambda} = 1$.

3.3 Isotope dependence

Besides ^{20}Ne there exist two other stable isotopes of neon, the bosonic ^{22}Ne and the fermionic ^{21}Ne, with natural abundance ratios of ^{20}Ne:^{21}Ne:^{22}Ne = 1:0.0030:0.102 [30]. We investigated the achievable beam flux of each of these by scanning the dye laser over a 2 GHz frequency range covering resonance lines of every isotope [31] and recording the resulting beam flux. Figure 8 shows the observed signal, with all of the isotopes indeed appearing. From the areas under the appropriate peaks we conclude that the ratios of maximum beam flux are ^{20}Ne*:^{21}Ne*:^{22}Ne* = $1{:}(0.0011 \pm 0.0002){:}(0.12 \pm 0.01)$, not far from their natural abundance ratios. The relatively low output of ^{21}Ne is easily explained by the fact that, due to its hyperfine structure, only part of such atoms can be manipulated at one time (in fact, only the $F = 7/2$ state can easily be laser cooled), while in addition laser cooling for this isotope leads to losses when there is no repumper laser present [19]. In the light of earlier experiments by Shimizu *et al.* [32], who observed that they could not trap ^{21}Ne* unless they supplied repumper light, the beam flux we achieve without it is somewhat remarkable. Given the maximum output we obtained with ^{20}Ne, the signals recorded imply that under optimum conditions the setup can deliver a flux of 7×10^7 metastable ^{21}Ne atoms/s. In our experience, this is quite sufficient for loading a magneto-optical trap with around 10^8 fermionic metastable atoms [25]. Of course, this value could easily be increased by using an enriched gas.

By locking the dye-laser on a saturated absorption signal for ^{22}Ne, we studied the spatial profile of the cold and intense beam of this isotope. As seen in Figure 9, which shows profiles for both ^{22}Ne and ^{20}Ne measured with the fourth wire scanner, the ^{22}Ne atomic beam has virtually the same width and divergence as the ^{20}Ne beam, and simply contains about seven times fewer atoms than the ^{20}Ne beam.

4 Discussion and conclusions

We have described the implementation of an extensive beam brightening scheme based on manipulation of atomic trajectories by radiation pressure forces. This technique is especially useful for metastable rare gases because of the low efficiency with which these species can be produced in discharge sources. Our setup contains three elements that are essential for reaching very high brilliance:

(1) a collimator that increases the atom flux,
(2) a slower that reduces both the average velocity and the velocity spread,
(3) and a compressor that increases the density by reducing the beam diameter.

The use of each one of these elements with metastable rare gas beams has been reported earlier. In most of these

cases, however, emphasis has been on reaching a high flux of slow atoms in order to load a large number of atoms into a magneto-optical trap (MOT). For such experiments, high brightness is not essential so that only a collimator and slower suffice. This combination does not create an atomic beam in the traditional sense of having a small diameter and small divergence, *i.e.*, having high brightness. Precise data on useful flux or brightness produced after slowing have not been published. In this case one could compare MOT loading rates, but this is somewhat out of the scope of the current paper.

In a separate paper [25], however, we will report on loading a MOT with our bright beam. Its small divergence allows us to pass the beam through two 8 mm diameter flow restrictions for differential pumping before entering the trapping chamber, ensuring very low background pressure. The low velocity of the beam makes it possible to slow the atoms down to the capture velocity of the MOT with a ≈20 mm long Zeeman slower positioned immediately before the trap. In combination with the small diameter of the beam, this results in a very high flux of atoms delivered directly within the spatial capture range of the MOT, which was limited to a diameter of 18 mm by the size of the trapping beams that we used. We have observed MOT loading rates of up to 3.6×10^{10} atoms/s, constituting nearly 65% of the total beam flux. Because of this high efficiency, we are able to trap up to 9×10^9 metastable ^{20}Ne atoms and 3×10^9 metastable ^{22}Ne atoms in our MOT under otherwise conventional trapping conditions. These numbers are substantially higher than reported by others [5,14,26,27] for brightened but not compressed metastable atomic beams.

Applications where high brightness as afforded by the use of a MOC is clearly profitable, *e.g.*, atom lithography, certain quantum optics experiments and loading hollow fiber guides, have been reported by Engels *et al.* [10], Koolen [4] and Dall *et al.* [12,33], respectively. In the latter two cases, the experimental setups used are based on virtually the same ideas as ours but use helium as the rare gas. The difficulties of manipulating helium, with its comparatively small linewidth, have led to beam fluxes that are smaller by a factor of 3 to 6 [4,12,33]. Baldwin and co-workers [12,33] report a final beam area of around 5 mm^2 and a divergence of 20 mrad, suggesting a somewhat smaller brightness was achieved. Koolen's setup produces a brightness of 1.0×10^{21} s^{-1}m^{-2}sr^{-1}, quite comparable to our result. Engels *et al.*, who also use neon, report a beam flux of 6×10^8 atoms/s, which is two orders of magnitude less than our current values, mostly due to the use of a less efficient collimator. Since, however, these authors achieved a much smaller beam diameter (70 μm) than we do as well as somewhat smaller divergence, their setup delivers a factor 3.3 higher phase space density and a factor 2.3 higher brilliance.

For alkali-metal beams, the highest brightness, 6.3×10^{21} Cs atoms s^{-1}m^{-2}sr^{-1} has been reported by Lison *et al.* [23]. Their setup uses a combination of a collimator, a slower and a lens plus re-collimator to produce a flux of 2.6×10^{10} Cs atoms/s. Comparing these numbers to our own, we find that they are nearly the same, notwithstanding the fact that we are forced to start out with a much lower brightness atom source. This again points out that very large gains in output are possible with beam brightening techniques which depend to a large degree on the efficiency of the collimator used.

Finally, there is still room for improvement of our results. For one, the use of a magneto-optic lens between slower and compressor could increase the final beam flux by a factor of ≈10 by effectively increasing the capture range of the compressor [4]. Also, outside of the region of strong Stern-Gerlach forces, sub-Doppler transverse cooling of the bright beam is possible in principle. Given the limits of such cooling mechanisms [19], a FWHM divergence of ≈2.4 mrad can be achieved leading to a gain in both brightness and brilliance of another factor of 10.

We are indebted to J.T.M. van Beek, W.J. Mestrom, V.P. Mogendorff, S.J.M. Kuppens, B.J. Claessens, and E.G.M. van Kempen for help with some of the experiments, to K.A.H. van Leeuwen for many helpful discussions, and to M.J. de Koning, L.A.H.M. van Moll and J.A.C.M. van de Ven for technical assistance. We thank A.E.A. Koolen for pointing out the effects of the Stern-Gerlach force to us. This work was supported by the Netherlands organization for Fundamental Research on Matter (FOM) and by the Royal Netherlands Academy of Arts and Sciences (KNAW).

References

1. B. Brutschy, H. Haberland, J. Phys. E **10**, 90 (1977).
2. For a recent comparison of metastable atom sources, see W. Lu *et al.*, Rev. Sci. Instrum. **72**, 2558 (2001).
3. M. Hoogerland *et al.*, Appl. Phys. B **62**, 323 (1996).
4. A. Koolen, Ph.D. thesis, Eindhoven University of Technology (2000); see also R.M.S. Knops *et al.*, Laser Phys. **9**, 286 (1999).
5. F. Shimizu, K. Shimizu, H. Takuma, Chem. Phys. **145**, 327 (1990).
6. A. Aspect *et al.*, Chem. Phys. **145**, 307 (1990).
7. A. Scholz *et al.*, Opt. Commun. **111**, 155 (1994).
8. J. Nellessen, J. Werner, W. Ertmer, Opt. Commun. **78**, 300 (1990).
9. M. Schiffer, M. Christ, G. Wokurka, W. Ertmer, Opt. Commun. **134**, 423 (1997).
10. P. Engels *et al.*, Appl. Phys. B **69**, 407 (1999).
11. D. Milic, M. Hoogerland, K. Baldwin, S. Buckman, Appl. Opt. **40**, 1907 (2001).
12. R. Dall, M. Hoogerland, K. Baldwin, S. Buckman, J. Opt. B **1**, 396 (1999); also C. R. Acad. Sci. IV **2**, 595 (2001).
13. W. Rooijakkers, W. Hoogervorst, W. Vassen, Opt. Commun. **123**, 321 (1996).
14. N. Herschbach, P. Tol, W. Hogervorst, W. Vassen, Phys. Rev. A **61**, 050702 (2000).
15. P. Tol *et al.*, Phys. Rev. A **60**, R761 (1999).
16. E. Rasel *et al.*, Eur. Phys. J. D **7**, 311 (1999).
17. G. Labeyrie *et al.*, Eur. Phys. J. D **7**, 341 (1999).
18. S. Nowak *et al.*, Appl. Phys. B **70**, 455 (2000).
19. H. Metcalf, P. van der Straten, *Laser cooling and trapping* (Springer, New York, 1999).

20. B. Sheehy, S. Shang, P. van der Straten, H. Metcalf, Chem. Phys. **145**, 317 (1990).
21. The term "lens" is used to accentuate the similarities with an optical lens. However, there are also some substantial differences, *e.g.*, the distance at which the atom trajectories are focused by a MOL is independent of the divergence of the impinging atomic beam.
22. W. Phillips, H. Metcalf, Phys. Rev. Lett. **48**, 596 (1982)
23. F. Lison, P. Schuh, D. Haubrich, D. Meschede, Phys. Rev. A **61**, 013405 (1999).
24. H. Hotop, "Atoms and Molecules", in *Atomic, Molecular and Optical Physics* (Academic Press, New York, 1996), Vol. 29b, p. 191.
25. S. Kuppens *et al.*, Phys. Rev. A (2001, accepted for publication).
26. A. Robert *et al.*, Science **292**, 461 (2001).
27. F.D. Santos *et al.*, Eur. Phys. J. AP **14**, 69 (2001).
28. R. Stas, Master's thesis, Eindhoven University of Technology, 1999, unpublished.
29. In the formulas we give here several factors of 2 appear compared to those in reference [23] because we define spatial and velocity spreads in terms of their FWHM rather than HWHM values.
30. *CRC Handbook of Chemistry and Physics*, edited by D.R. Lide, 72nd edn. (CRC Press, Boca Raton, 1991).
31. L. Julien, M. Pinard, F. Laloe, J. Phys. Lett. (Paris) **41**, L479 (1980).
32. F. Shimizu, K. Shimizu, H. Takuma, Phys. Rev. A **39**, 2758 (1989).
33. M. Hoogerland, K. Baldwin, private communication.